Lewis Acid Coordination Complexes of Polymers. 2. Computational Modeling of Single-Chain and Aggregate Structures of Rigid-Rod Poly(*p*-phenylenebenzobisthiazole)

Michael F. Roberts,[†,⊥] Samson A. Jenekhe,[*,†,‡] Alan Cameron,[§,∥] Martin McMillan,[§] and Jerry Perlstein[‡]

Department of Chemical Engineering and Center for Photoinduced Charge Transfer, University of Rochester, Rochester, New York 14627-0166, and Eastman Kodak Company, Rochester, New York 14650

Received July 13, 1993. Revised Manuscript Received February 16, 1994[⊗]

Computational modeling of the molecular, electronic, and one-dimensional-aggregate structures of oligomers of poly(*p*-phenylenebenzobisthiazole) (PBZT) and its 1:4 (repeating unit:Lewis acid) complexes has been made and used to explain previous experimental results. In the calculations the structure of PBZT was approximated by its monomeric model compound (2,6-diphenylbenzo[1,2-*d*:4,5-*d'*]bisthiazole) (t-DBZT), dimer, and trimer and the PBZT complexes by the $AlCl_3$ complexes of t-DBZT and the dimer. Geometry optimization, carried out by using MM2 and MOPAC-PM3, shows that PBZT has an essentially planar structure whereas the t-DBZT complex is sterically congested, exhibiting out-of-plane phenylene ring twists of 62°. Increased congestion in the dimer complex results in even larger dihedral angles. Calculations of the partial atomic charges with MOPAC-ESP indicate that the Lewis acid–base reactions involve electron transfer from the base (polymer) to the Lewis acid. INDO/S calculations are used to explain the experimentally observed absorption spectra. Complexation has two opposing effects on optical absorption: a blue shift of the absorption edge and maximum is induced by steric congestion, while participation of the metal halide in electron delocalization produces a compensating red-shift. Monte carlo (MC) simulations of the one-dimensional aggregate structures of PBZT reveal that it forms very tightly packed structures with perpendicular interchain distances of typically 3.3–3.5 Å, in accord with experiment. MC simulations of the aggregate structures of the complexes reveal very inefficiently packed structures with large unfillable voids between the molecules. The computational modeling results explain the observed properties of Lewis acid coordination complexes of PBZT qualitatively, including solubility in organic solvents, formation of liquid-crystalline solutions at high critical concentrations, and extremely low glass transition temperature (T_g).

Introduction

In a previous paper[1] we presented studies of the coordination complexes of poly(*p*-phenylenebenzobisthiazole) (PBZT) with group III metal halide Lewis acids. In these complexes the metal halide (e.g., BCl_3, $AlCl_3$, $GaCl_3$) is coordinately bonded to nitrogen and sulfur heteroatoms in the polymer backbone. These complexes are highly soluble in organic solvents, in contrast to the pure PBZT which is virtually insoluble except in concentrated acids. The solid PBZT/$GaCl_3$ complex also exhibits a low glass transition temperature (26–30 °C) compared to the pure PBZT which shows no discernible glass transition or melting point below its decomposition temperature (>700 °C in nitrogen).[1,2]

In this paper we seek a molecular level understanding of the effects of complexation on the structure and properties of PBZT through theoretical calculations on idealized structures of PBZT and its complexes. Specifically, we have sought to answer two main questions: (1) What are the effects of Lewis acid complexation on (a) molecular structure and conformation and (b) electronic structure of PBZT? (2) How does structure account for the observed solution- and solid-state properties of the complexes? To answer these questions we proceeded as follows. To address 1a we carried out MNDO-PM3[3a] and MM2[4] energy minimizations, using MOPAC[3b] and MACROMODEL,[5] of a model compound of PBZT, viz., 2,6-diphenylbenzo[1,2-*d*:4,5-*d'*]bisthiazole (t-DBZT), the PBZT dimer, the PBZT trimer, the 1:4 t-DBZT:$AlCl_3$ complex, and the 1:8 PBZT dimer:$AlCl_3$ complex. The chemical structures of these molecules are shown in Figure 1. These procedures yielded energy-minimized structures for the isolated molecules of each. The MM2 force field was used

† Department of Chemical Engineering.
‡ Center for Photoinduced Charge Transfer.
§ Eastman Kodak Co.
* To whom correspondence should be addressed.
⊥ Present address: Gillette Co., Boston R&D Laboratory, 1 Gillette Park, Boston, MA 02127.
∥ Present address: SynPhar Laboratories, Inc., No. 2 Tarho Alberta Center, 4290-91A Street, Edmonton, Alberta, Canada T6E 5V2.
⊗ Abstract published in *Advance ACS Abstracts*, April 1, 1994.
(1) Roberts, M. F.; Jenekhe, S. A. *Chem. Mater.* **1993**, *5*, 1744–1754.
(2) References to earlier work on PBZT by our laboratory and others are given in ref 1.
(3) (a) Stewart, J. J. P. *J. Comput. Chem.* **1989**, *10*, 209–220. (b) Stewart, J. J. P. MOPAC Version 6.0, Quantum Chemical Program Exchange, Indiana University, Bloomington, IN, 1990.
(4) Allinger, N. L. *J. Am. Chem. Soc.* **1977**, *99*, 8127–8134.
(5) Mohamadi, F.; Richards, N. G. J.; Guida, W. C.; Liskamp, R.; Lipton, M.; Caufield, C.; Chang, G.; Hendrickson, T.; Still, W. C. *J. Comput. Chem.* **1990**, *11*, 440.
(6) (a) Perlstein, J. *J. Am. Chem. Soc.* **1992**, *114*, 1955–1963. (b) Perlstein, J. *J. Am. Chem. Soc.* **1994**, *116*, 455–470. (c) Perlstein, J. *Chem. Mater.* **1994**, *6*, 319–326.

0897-4756/94/2806-0658$04.50/0

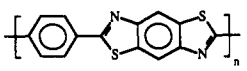

(a)

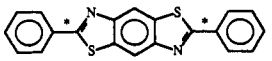

(b)

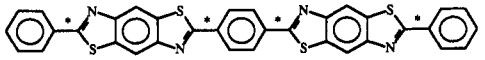

(c)

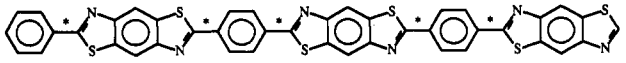

(d)

Figure 1. Molecular structures of (a) PBZT, (b) t-DBZT, (c) phenyl end-capped PBZT dimer, and (d) PBZT trimer, used in the calculations. C–C single bonds about which rotations are considered in the Monte Carlo simulations are indicated by an asterisk.

for t-DBZT, the PBZT dimer, and the PBZT trimer. The resulting molecular geometries were subsequently used in Monte Carlo simulations of aggregate structures. MM2 has not been parametrized for aluminum atoms and so MNDO-PM3 was used in energy minimization of the single molecule complex structures. To address 1b, the MOPAC electrostatic potential (ESP) method was used to calculate partial atomic charges for t-DBZT and its 1:4 complex with $AlCl_3$. INDO/S[7] calculations of the absorption spectra of individual molecules were carried out, and the results obtained were used to interpret experimentally observed spectra. To answer question 2, we used Perlstein's Monte Carlo cooling method[6] to predict one-dimensional aggregate structures for t-DBZT, the PBZT dimer, the trimer, and the $AlCl_3$ complexes of t-DBZT and the PBZT dimer. Although the method is described in detail elsewhere,[6] a brief review of the overall procedure and terminology here will facilitate the discussion. The method is based on Kitaigorodskii's work,[8] as developed by Scaringe and Perez.[9] The basic tenet is that three-dimensional crystal structures are made up of stacks of stable two-dimensional layers which in turn are composed of stable one-dimensional aggregates of the individual molecules. Analysis of a large number (5000) of structures showed that 92% of the time, the molecules in these one-dimensional aggregates are related by one of four symmetry operations: *translation*, *glide*, *screw*, or *inversion*, with only one symmetry-independent molecule per identity period. The goal of the reported work[6] was to enable quantitative prediction of two-dimensional layer structures and three-dimensional crystal structures by first generating the most probable one-dimensional aggregates. Up to now, it has been shown that it is possible to quantitatively predict the geometry of these one-dimensional aggregates for real systems using very few assumptions.[6] These structures always lie close in energy to the global minimum aggregate structures. Prediction of the low-energy aggregates involves a Monte Carlo cooling procedure to locate local minima for five molecule aggregates, given only the molecular valence geometry. Our use of the method here is to study aggregate structures for oligomers of PBZT and their Lewis acid coordination complexes and to interpret polymer and complex physical properties in terms of the chain packing.

Methods

(A) Molecular Structures and Conformations. Preliminary coordinates for the t-DBZT molecule were obtained from the crystal structure for this compound.[12] Energy minimization for this molecule was then done using Allinger's MM2 force field[4] in MACROMODEL,[5] and the coordinates obtained for all atoms were transferred to CHEM-X[10] for viewing and for use in Monte Carlo simulations. The PBZT dimer molecule was constructed from two molecules of t-DBZT (with appropriate atom deletions) followed by energy minimization as for t-DBZT. The PBZT trimer was constructed in a similar fashion. An approximate structure for the 1:4 t-DBZT:$AlCl_3$ complex was constructed by attaching tetrahedral $AlCl_3$ molecules to the sulfurs and nitrogens of PBZT. MOPAC[3b] was then used to minimize the energy of the structure using the PM3 Hamiltonian[3a] and an eigenvector-following routine (EF) to search the geometry. An optimized geometry for the 1:8 PBZT dimer:$AlCl_3$ complex was similarly obtained.

CHEM-X and MACROMODEL were used on a VAX 8600 with an Evans and Sutherland 3-D graphics terminal. MOPAC was compiled and run on an IBM RS/6000 workstation with a UNIX operating system.

(B) Electronic Structures. Partial atomic charges for t-DBZT and the 1:4 t-DBZT:$AlCl_3$ complex and $AlCl_3$ molecules were calculated with MOPAC using the keywords ESP and NSURF = 4,[11a] and the optimized geometries were obtained as described above. Spectroscopic calculations used the INDO/S method of Zerner et al.[7] For a qualitative comparison of the results the spectra were simulated[11b] assuming Lorentzian line shapes of 3000 cm^{-1} width and a spectral resolution of 100 cm^{-1}.

(C) One-Dimensional Aggregate Structures. Complete details of the procedure used to run Monte Carlo simulations on one-dimensional aggregates have been provided elsewhere.[6] Here we give only an overview of the calculations with details unique to the structures under study.

Monte Carlo simulations were carried out to find energy-minimum structures for one-dimensional aggregates of the following: t-DBZT, PBZT dimer, PBZT trimer, 1:4 t-DBZT:$AlCl_3$ complex, and 1:8 PBZT dimer:$AlCl_3$ complex. The PBZT trimer and the PBZT dimer complex were the largest oligomers of PBZT and their complexes that were studied, due to computational constraints. Five-molecule aggregates of each were constructed in CHEM-X by replication of the appropriate starting structure four times. For t-DBZT and the PBZT dimer and trimer, only translation aggregates were considered since it is known from experiment that the lowest energy one-dimensional aggregates for t-DBZT and PBZT have translation symmetry (see Appendix A and refs 12 and 13). For the complexes however, the symmetry is not obvious and *translation*, *glide*, *screw*, and *inversion* aggregates were considered.

Energy Computation. In an infinite (instead of five-molecule) aggregate, the binding energy per molecule is equal to one-half the energy of any one molecule. We calculate the binding energy as one-half the energy of the center molecule in a five-

(7) (a) Ridley, J.; Zerner, M. *Theor. Chim. Acta* **1973**, *32*, 111–134. (b) Bacon, A. D.; Zerner, M. *Theor. Chim. Acta* **1979**, *53*, 21–54.

(8) Kitaigorodskii, A. I. *Organic Chemical Crystallography*; Consultants Bureau: New York, 1961.

(9) Scaringe, R. P. In *Electron Crystallography of Organic Molecules*; Fryer, J. R., Dorset, D. L., Eds.; Kluwer: Dordrecht, 1990; pp 85–113. (b) Scaringe, R. P.; Perez, S. *J. Phys. Chem.* **1987**, *91*, 2394–2403.

(10) CHEM-X is a molecular modeling program developed and distributed by Chemical Design Ltd., Roundway House, Cromwell Park, Chipping Norton, Oxon OX7 5SR, UK.

(11) (a) Eilers, J., private communication, (b) Canuto, S., private communication.

(12) Wellmann, M. W.; Adams, W. W.; Wolff, R. A.; Dudis, D. S.; Wiff, D. R.; Fratini, A. V. *Macromolecules* **1981**, *14*, 935–939.

(13) Fratini, A. V.; Lenhert, P. G.; Resch, T. J.; Adams, W. W. *Mater. Res. Soc. Symp. Proc.* **1989**, *134*, 431–445.

molecule aggregate. Inclusion of nearest and next-nearest neighbor molecules accounts for the binding energy of a molecule to a good approximation.[6]

Contributions to the total energy (E_T) come from three sources in the present model: (a) a nonbonding van der Waals term E_{nb}, (b) an electrostatic term E_{el}, and (c) an intramolecular term E_{intra}. Thus

$$E_T = E_{nb} + E_{el} + E_{intra} \quad (1)$$

The nonbonding term is that used in Allinger's MM2 force field.[4] For two atoms i and j in different molecules separated by a distance r_{ij} this is

$$E_{ij}^{nb} = A_{ij}\left[(2.90 \times 10^5)\exp\left(\frac{-12.50 r_{ij}}{B_{ij}}\right) - 2.25\left(\frac{B_{ij}}{r_{ij}}\right)^6\right] \quad (2)$$

where

$$A_{ij} = (A_i A_j)^{1/2} \quad (3)$$

$$B_{ij} = B_i + B_j \quad (4)$$

The total nonbonded energy for an aggregate is then

$$E_{nb} = {}^1/_2 \sum_{i,j} E_{ij}^{nb} \quad (5)$$

where the summation is over all atoms i on the center molecule and all atoms j on the other four molecules in the aggregate. The parameters A_i and B_i were taken from MACROMODEL for all atoms except aluminum. Unfortunately no such parameters are available for aluminum, and we therefore calculated approximate values. Details of the calculation are given in Appendix B.

The electrostatic term was approximated by a summation of Coulombic terms where for atoms i and j with charges q_i and q_j, separated by a distance r_{ij}

$$E_{ij}^{el} = q_i q_j / \epsilon r_{ij} \quad (6)$$

where ϵ is a distance dependent dielectric constant equal to $\epsilon_0 r_{ij}$ with $\epsilon_0 = 1.0$. The total electrostatic term is

$$E_{el} = {}^1/_2 \sum_{i,j} E_{ij}^{el} \quad (7)$$

where again the summation is over all atoms i on the center molecule and all atoms j on the other four molecules in the aggregate. The atomic charges for this calculation were approximated using Gasteiger's procedure.[14] Gasteiger's method was not formulated to handle conjugated systems and indeed gives poor agreement with, for example, ESP charges from MOPAC for the molecules under study. However, in all cases the electrostatic term E^{el} is not large compared to E^{nb} as will be evident later, and since Coulombic forces are long range they vary only slowly with the structural variables, compared to nonbonded interactions, and so are not structure determining. Therefore, although the charge distribution is only crudely represented by Gasteiger charges, E^{el} can still be estimated using them with sufficient accuracy. As a test of this assumption we ran Monte Carlo simulations for the 1:4 t-DBZT:$AlCl_3$ complex translation aggregate first using Gasteiger charges and then again using ESP charges to calculate the electrostatic term. Examination of the lowest energy structures showed that the respective global minimum energies were −18.86 and −19.17 kcal/mol ranging to −16.58 and −17.16 kcal/mol for the next 10 lowest energy structures. In the Gasteiger case E^{el} ranged from 3.11 to 3.49 kcal/mol and in the ESP case from 3.35 to 4.05 kcal/mol. More significantly, each of the 10 lowest energy "Gasteiger" aggregates corresponded to an "ESP" aggregate with translation distance within 0.04 Å and all angles with the z axis within 1°. Thus we use Gasteiger charges for calculation of the electrostatic energies because of simplicity and computational speed, and ESP charges which are more accurate (but take considerably more cpu time), to analyze the electron redistribution when t-DBZT is complexed with $AlCl_3$.

One of us (J.P.) recently added an intramolecular term to the above model.[6c] This energy is added to the nonbonded and electrostatic energies and accounts for conformational changes induced in molecules which are not truly rigid, when they pack in aggregates. Specifically, dihedral angles are identified in the starting molecular structures which are randomly changed along with the other structural variables during the Monte Carlo simulations and the induced change in intramolecular energy is calculated and added to E_T. In t-DBZT and the PBZT dimer and trimer molecules we included the dihedral angles defined about the C–C bonds linking phenylene and benzobisthiazole moieties. These bonds are known to exhibit low rotational barriers (on the order of 2 kcal/mol[15,16]) and so the dihedral angles are likely to be affected by intramolecular interactions. The torsional energy E_ω about such a bond ω is calculated from Allinger's MM2 model[4] as follows:

$$E_\omega = \frac{V_1}{2}(1 + \cos\omega) + \frac{V_2}{2}(1 - \cos 2\omega) + \frac{V_3}{2}(1 + \cos 3\omega) \quad (8)$$

V_1, V_2, and V_3 are torsion barrier heights. E_ω is calculated for each rotatable bond in a molecule. For example, for t-DBZT this involves the two C–C bonds. Intramolecular nonbonding and electrostatic terms are calculated using eqs 2 and 6 with subscripts i and j in these equations representing different atoms on the same molecule this time with $i < j$ to avoid double counting of interactions, and only 1,4 interactions and beyond are included. The intramolecular energy term E_{intra} is calculated as the change in intramolecular energy, made up of torsional, nonbonding, and electrostatic terms, induced by the change in conformation from the starting structure. In this respect it is important that the starting structure be a low-energy structure (i.e., an intramolecular local energy minimum). E_{intra} contributions were included in Monte Carlo simulations for t-DBZT, and PBZT dimer and trimer. For the $AlCl_3$ complexes, however, they were not and the total energy E_T was calculated from eq 1 with E_{intra} equal to zero. The implicit assumption that the complex structures are rigid is necessary due in part to the absence of accurate MM2 parameters for aluminum and the fact that the approximate 3-fold symmetry for the $AlCl_3$ rotation precludes any other geometry.

Monte Carlo Simulations. The Monte Carlo algorithm used is described in detail in ref 6a. In a typical simulation, the apparent global energy minimum for a five-molecule aggregate is found along with energetically nearby local minima. This is done by random sampling of aggregate structures. Importance sampling using the Metropolis algorithm[17] coupled with a heuristic cooling schedule allows the system to move out of local energy wells to new minima in a computationally efficient manner and in reasonable times. The results obtained consist of local minimum energies and their geometries. The minima were ordered according to total energy and sorted into groups or "orders" of minima with very close geometries according to Perlstein's prescriptions for root-sum-square (RSS) differences.[6] RSS cutoff values of 10 were used to sort the results into orders. The lowest energy entry in each order was considered to represent the geometry of that particular order. The simulations were run on the IBM RS/6000 workstation. The energy minimum aggregate geometries were transferred to the VAX 8600 for viewing with CHEM-X.

Results

Molecular Structures. The coordinates obtained for the MM2 minimized starting geometry of t-DBZT, PBZT dimer and trimer are given in the supplementary material and the atom numbering scheme for t-DBZT molecule is given in Figure 2a. The molecule is predicted to be linear and flat. The phenylene end groups exhibit 0° of twist

(14) Gasteiger, J.; Marsili, M. *Tetrahedron* **1980**, *36*, 3219–3228.

(15) Yang, Y.; Welsh, W. J. *Macromolecules* **1990**, *23*, 2410–2412.

(16) Welsh, W. J.; Yang, Y. *Comput. Polym. Sci.* **1991**, *1*, 139–150.

(17) Binder, K. *Topics in Current Physics*, 2nd ed.; Springer-Verlag: New York, 1987; Vol. 36, pp 1–36.

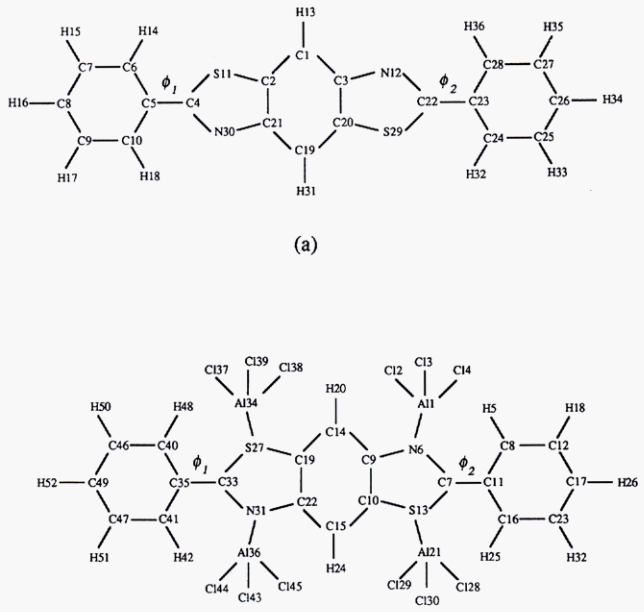

Figure 2. Atom numbering schemes used for (a) t-DBZT and (b) 1:4 t-DBZT:$AlCl_3$ complex. Rotations about the C–C single bonds are measured by the dihedral angles ϕ_1 and ϕ_2 indicated, which the phenyl rings make with the plane of the benzobisthiazole moiety.

out of the plane of the bisthiazole ring (ϕ_1, ϕ_2 = 0.00). The closeness of this geometry to the actual global energy minimum structure is dependent on the accuracy of the MM2 parameters and minimization procedure. It has been reported several times in the literature[15,16,18–20] that the energy barrier to rotation about the C4–C5 and C22–C23 bonds is very low. Welsh and Yang[16] reported AM1 calculations indicating that the energy minimum is where the dihedral angle (ϕ) is 21° with energy barriers of 0.036 and 2.17 kcal/mol to the coplanar (ϕ = 0°) and perpendicular (ϕ = 90°) geometries, respectively. All other reports gave similar values.[15,18–20] Although the values of ϕ for the global energy minimum have generally been predicted to be in the range 21–29°, clearly, no molecular model or semiempirical model used can be considered accurate enough to locate the exact minimum with such a shallow potential well. For example, MNDO is known to overestimate core repulsions,[21] AM1[21] can be expected to give errors on the order of 6 kcal/mol for heats of formation and on the order of 1.7 kcal/mol for rotational barriers, and molecular mechanics models such as that of Scott and Scheraga[22] or MM2[4] are of similar accuracy. We rationalize that (1) our MM2 result is of comparable reliability to earlier reports and (2) the preponderance of evidence from varied calculations indicates that the true global minimum is probably somewhere in the region of ϕ = 0–30°. Regardless of the values of the dihedral angles in an energy-minimized single molecule, their values in real crystal structures, in aggregates, and in solution will probably be determined by interactions with the surroundings, i.e., with other molecules or solvent, since the barriers to bond rotation are so low compared to such forces. We will discuss this point again later in relation to our aggregate structure calculations.

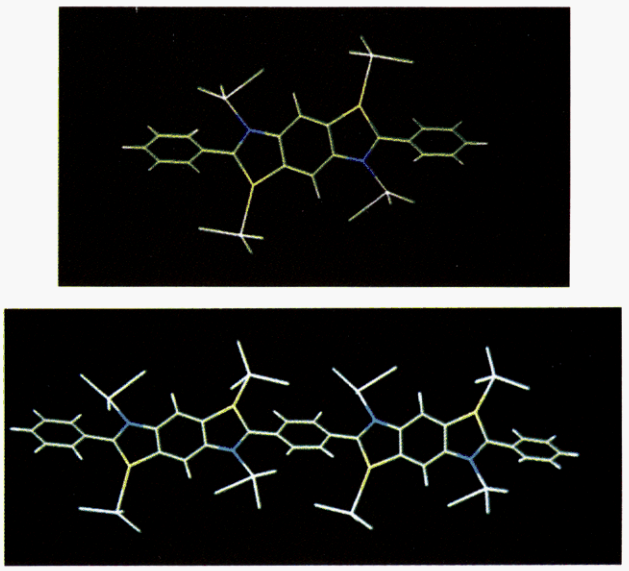

Figure 3. MOPAC-PM3 optimized structures for (a, top) the 1:4 t-DBZT:$AlCl_3$ complex and (b, bottom) the 1:8 PBZT dimer:$AlCl_3$ complex.

Energy minimization for the PBZT dimer molecule (Figure 1c) using MM2 predicted ϕ = 22.8° on average, and similar twists from coplanarity were obtained for the PBZT trimer (Figure 1d). The coordinates for both structures are available as supplementary material (see paragraph at end of paper). Polymerization is predicted to have little effect on the basic repeat unit geometry. For t-DBZT the length of the polymer repeat unit (i.e., C5–C26) is 12.50 Å, changing to 12.53 Å for the trimer. These values are very close to the reported value of 12.51 Å for the high molecular weight PBZT from X-ray diffraction studies.[13] Only a very slight deviation from a linear structure is seen for the trimer. The end-to-end distance for three repeat units is predicted to be 37.17 Å, just less than 3 times the single repeat unit length (37.59 Å).

PM3 optimized coordinates for the 1:4 t-DBZT:$AlCl_3$ and the 1:8 PBZT dimer:$AlCl_3$ complex are also presented in the supplementary material with the corresponding atom numbering scheme in Figure 2b. CHEM-X visualization of the structures is shown in Figure 3. In the t-DBZT complex, coordination of aluminum to nitrogen and sulfur results in N–Al and S–Al interatomic distances of 1.90 and 2.59 Å, respectively. The van der Waals radii of nitrogen and sulfur are 1.55 and 1.80 Å, respectively, and an approximate value of 2.51 Å has been given for aluminum.[23] Thus interatomic N–Al and S–Al distances are significantly lower than the sum of the van der Waals radii (4.06 and 4.31 Å, respectively), and the interactions are therefore significant. PM3 calculations predict a favorable enthalpy change ΔH = –32.86 kcal/mol (calculated from individual heats of formation) for the complexation reaction: t-DBZT + $4AlCl_3$ = t-DBZT:$(AlCl_3)_4$. A PM3 optimization of $AlCl_3$ yielded a triangular planar structure with Cl–Al–Cl bond angles of 120°. (Actually, pure $AlCl_3$ crystallizes as the dimer Al_2Cl_6[24]). Coordination

(18) (a) Welsh, W. J.; Bhaumik, D.; Mark, J. E. *Macromolecules* **1981**, *14*, 947–950. (b) Bhaumik, D.; Welsh, W. J.; Jaffe, H. H.; Mark, J. E. *Macromolecules* **1981**, *14*, 951–953.

(19) Bhaumik, D.; Mark, J. E. *J. Polym. Sci., Polym. Phys. Ed.* **1983**, *21*, 1111–1118.

(20) Farmer, B. L.; Wierschke, S. G.; Adams, W. W. *Polymer* **1990**, *31*, 1637–1648.

(21) Dewar, M. J. S.; Zoebisch, E. G.; Healy, E. F.; Stewart, J. J. P. *J. Am. Chem. Soc.* **1985**, *107*, 3902–3909.

(22) Scott, R. A.; Scheraga, H. A. *J. Chem. Phys.* **1965**, *42*, 2209–2215.

(23) Bondi, A. *J. Phys. Chem.* **1964**, *68*, 441–451.

to nitrogen results in a tetrahedral or less planar structure with predicted Cl–Al–Cl bond angles of 96, 102, and 123°. At sulfur, $AlCl_3$ is less distorted from triangular planarity with bond angles of 116, 117, and 122°. Steric congestion about the nitrogens and sulfurs caused by coordination is evident in both complexes of Figure 3. Large out-of-plane deformations of the phenylene rings are induced. In the 1:4 t-DBZT:$AlCl_3$ complex the phenylene rings are twisted (ϕ_1, ϕ_2=) 62° out of the plane of the benzobisthiazole ring. Increased steric congestion about the central phenylene ring in the 1:8 PBZT dimer:$AlCl_3$ complex leads to twists of 72 and 100°. Despite these deformations of the molecular backbones, the complexes are predicted to retain the linear rigid-rod topology characteristic of PBZT. The repeat unit length in the 1:4 t-DBZT:$AlCl_3$ complex (C11–C49 in Figure 2b) is 12.58 Å and the end-to-end distance of two repeat units in the dimer complex is close to twice this at 25.27 Å.

The energy barriers to achieving a planar conformation are probably large in both complexes of Figure 3, compared to the t-DBZT and PBZT dimer. Interatom spacings about the complexation sites are already quite small compared to van der Waals radii even with the large induced twist angles (e.g., Al36–H42 = 2.56 Å in Figure 2b). The necessary MM2 parameters for stretching, bending, stretch–bending, and torsion interactions for aluminum are not available, and so we could not carry out a conformational analysis for the complexes nor include the dihedral angles in the Monte Carlo simulations with any reasonable hope of accuracy. We therefore assumed rigid geometries for both structures.

Partial Atomic Charges and Electronic Structures. The method of Besler et al.[25] is used in the MOPAC program (by specifying ESP) to estimate charges directly from the wave functions. The calculated partial atomic charges in t-DBZT and the 1:4 t-DBZT:$AlCl_3$ complex are given in the supplementary material. A similar calculation for $AlCl_3$ gave charges of 1.0614 for aluminum and –0.3393, –0.3836 and –0.3835 (all charges referred to here are in units of the electron charge) for the chlorines. Analysis of these charges gives a picture of the electron redistribution which takes place on complexation. Coordination of aluminum at nitrogen results in electron withdrawal from t-DBZT. $AlCl_3$ which coordinates to N12 in Figure 2a gains electron density (–0.6538 charge), most of which (–0.5855) resides on aluminum, the remainder being distributed among the chlorines. At N30 the net $AlCl_3$ charge decreases by 0.6190, this time with slight electron withdrawal by aluminum from the chlorines (–0.0316 charge) too. Most of the electron donation is by the nitrogens although there is a charge redistribution throughout the molecule. Referring again to Figure 2a N12 donates a charge of –0.6591 and N30 donates –0.5810. Changes in electron density at adjacent carbons are less dramatic. For example there are the following changes in atomic charges on complexation: C22, –0.1591; C23, –0.0588; C3, –0.3325; C20, +0.2625; C1, –0.1865. The electron withdrawal at sulfur is much less than at nitrogen. $AlCl_3$ complexed to S11 gains 0.0786 electron and 0.0957 electron is transferred at S29. As in the case of coordination to the nitrogens, most of this electron density is withdrawn from the sulfurs and resides on the aluminum atoms. Aluminum coordinated to sulfur also appears to increase in electronegativity relative to chlorine, Al21 and Al34 (Figure 2b) withdrawing 0.2371 and 0.1344 electron from attached chlorines, respectively. The dipole moments evaluated from ESP point charges are 1.3201 and 0.4223 D respectively for t-DBZT and $AlCl_3$. The predicted dipole moment for 1:4 t-DBZT:$AlCl_3$ is much higher at 6.2549 D.

Table 1. π–π^* Absorption Maxima (λ_{max}) and Optical Bandgaps (E_g) for t-DBZT and Its Complexes with Lewis Acids. Data Taken from Ref 1

	λ_{max} (nm)	E_g (eV)
t-DBZT[a,b]	346,363	3.06 (405 nm)
t-DBZT/$AlCl_3$ in nitromethane[c]	365	3.13 (396 nm)
t-DBZT/$GaCl_3$ in nitromethane[c]	365	3.13 (396 nm)
t-DBZT in dichloromethane[a,c]	347	3.28 (378 nm)

[a] Multiple peaks were resolved in the π–π^* absorption band; details are given in ref 1. [b] Crystalline material supported in a nylon 66 matrix. [c] Solution concentrations of t-DBZT were approximately 10^{-5} M.

In a previous paper[1] we presented the absorption spectra for PBZT, t-DBZT, and their complexes. For PBZT, the optical bandgap (i.e., the low-energy band edge of the π–π^* transition of the absorption spectrum) is 2.53 eV (491 nm), and this is blue-shifted by only 0.03 eV (6 nm) and 0.02 eV (5 nm) in the solid PBZT/$AlCl_3$ and PBZT/$GaCl_3$ complexes, respectively. The π–π^* absorption maximum (λ_{max}) for PBZT is at 438 nm with a smaller shoulder peak at 468 nm. The respective λ_{max} values for the $AlCl_3$ and $GaCl_3$ complexes are 433 and 434 nm. Data for t-DBZT and its complexes are presented in Table 1. The π–π^* absorption band of crystalline t-DBZT is only slightly blue-shifted in the dissolved $AlCl_3$ and $GaCl_3$ complexes. There is a larger blue-shift of this band for t-DBZT in dichloromethane.

In light of the predicted molecular geometries discussed in the previous section, the reasons behind the effects of complexation on the absorption spectra are not obvious. Specifically, it seems strange that the large induced dihedral angles in the t-DBZT and PBZT dimer complexes do not cause larger blue-shifts of the main (lowest energy) bands. Welsh and Yang[16] have shown that the bandgap (E_g) of PBZT is very sensitive to ϕ, and they predict an increase of 0.27 eV in E_g between $\phi = 0°$ and $\phi = 90°$. We carried out INDO/S calculations for several structures to investigate this issue.

Figure 4 shows the simulated absorption spectra for t-DBZT and the PBZT dimer. Each molecular geometry was that obtained by minimization of the intramolecular energy using MACROMODEL, as described earlier. For t-DBZT the calculated peaks are at 210 and 348 nm. Examination of the orbitals showed that the 210-nm band is due to a localized excitation around the phenylene rings and the 348-nm band arises from a π–π^* transition delocalized throughout the molecular structure. In the dimer these bands are red-shifted to 218 and 392 nm. A simulation was also run for the dimer molecule with the same geometry as the molecule of Figure 4b (i.e., the energy-minimized dimer structure) except that dihedral angles of 90° were induced about the C–C bonds linking the central phenylene ring to the rest of the molecule. This resulted in a blue-shift of the low-energy absorption to 344 nm, relative to Figure 4b corresponding to an increase of 0.44 eV in the bandgap. This suggests that the red-shift of the 348-nm band of t-DBZT to 392 nm in the PBZT dimer is due mainly to effects of conjugation and demonstrates the importance of the dihedral angles to electronic structure.

(24) Thomas, C. A. *Anhydrous Aluminum Chloride in Organic Chemistry*; Reinhold Publishing Company: New York, 1941; pp 867–868.

(25) Besler, B. H.; Merz, K. M.; Kollman, P. A. *J. Comput. Chem.* **1990**, *11*, 431–439.

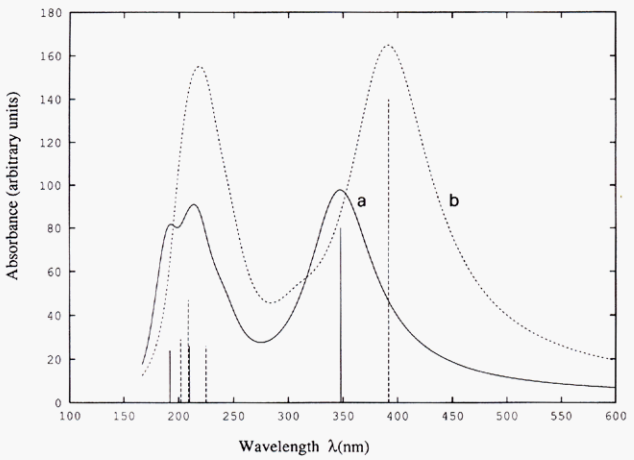

Figure 4. Simulated absorption spectra for single molecules of (a) t-DBZT of (b) PBZT dimer, having energy-minimized structures obtained with MACROMODEL.

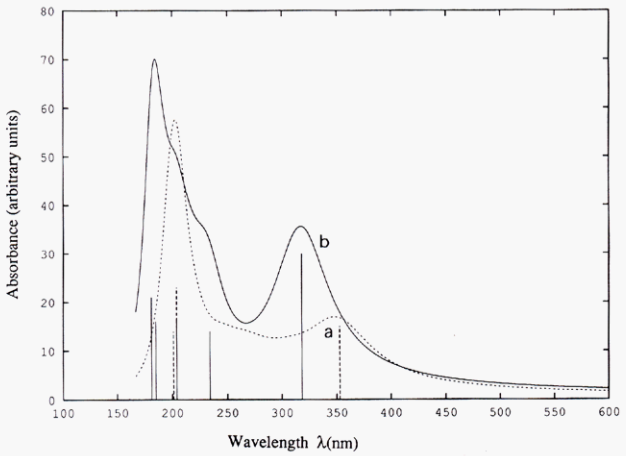

Figure 5. Simulated absorption spectra for single molecules of (a) 1:4 t-DBZT:$AlCl_3$ complex with MOPAC-PM3 optimized geometry and (b) t-DBZT with a molecular geometry obtained by removing Al and Cl atoms from the structure used in (a).

Figure 5a shows the absorption spectrum calculated for the geometry optimized structure of the 1:4 t-DBZT:$AlCl_3$ complex. The coordinates for this molecular geometry are presented in the supplementary material. The absorption maxima are at 204 and 353 nm. The results described above for the effect of dihedral angles on conjugation in the PBZT dimer led us to expect blue shifts in the absorption spectra of t-DBZT or other PBZT oligomers with increased dihedral angles in the molecular backbone. It was thus surprising that the 348-nm absorption of t-DBZT was not significantly blue-shifted in the complex since the dihedral angles about the C7–C11 and C33–C35 bonds (Figure 2b) are 62° whereas the t-DBZT structure used to calculate the spectrum of Figure 4a was essentially planar. We therefore attempted to estimate the effects of the coordinated $AlCl_3$ moieties on the absorption spectrum. Figure 5b shows the simulated spectrum for an uncomplexed t-DBZT molecule but with the geometry of the complex, i.e., with dihedral angles of 62°. The spectrum shows the expected blue-shift due to decreased conjugation. The absorption maxima are at 185 and 318 nm.

This gives the interesting prediction that despite the large dihedral angles induced by coordination of $AlCl_3$, there is not necessarily any blue-shift of the π–π^* absorption. This is indeed what is seen experimentally, i.e., the very small blue-shifts of λ_{max} and E_g on complexation of t-DBZT and PBZT. Also, the large blue-shift of t-DBZT in dichloromethane suggests that t-DBZT is highly nonplanar in this solvent.

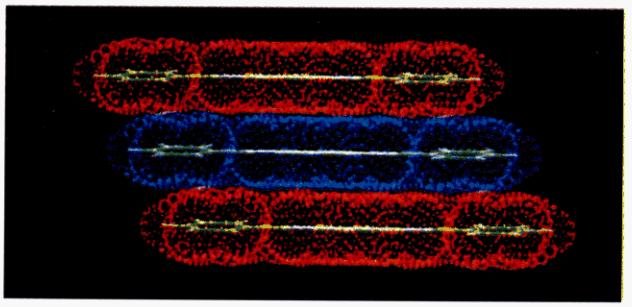

Figure 6. Three molecules of t-DBZT with the global energy minimum geometry viewed along the stacking direction (translation repeat = 3.79 Å). The surfaces shown are Connolly surfaces of the molecules computed from the van der Waals radii of the individual atoms.

Table 2. Lowest Energy Translation Aggregate Geometries and Energies for t-DBZT, PBZT-Dimer, and PBZT-Trimer

structure	θ_{iz}[a]	θ_{jz}[a]	θ_{kz}[a]	t[b]	E_{el}[c]	E_{nb}[c]	E_{intra}[c]	E_T[c]
t-DBZT	96.08	64.88	154.05	3.79	0.19	−17.95	0.05	−17.71
dimer	76.23	115.71	150.34	3.88	0.03	−32.59	−0.22	−32.78
trimer	101.50	62.39	149.70	4.00	−0.16	−42.04	0.42	−41.78

[a] Tilt angle (in degrees) in the i, j, or k direction (rotating axes) with respect to the z axis (stationary). [b] Translation repeat distance (along the z axis) in angstroms. [c] Energy in kcal/mol as defined by eq 1.

Monte Carlo Simulation of Aggregate Structures. (*A*) *t-DBZT, PBZT Dimer, and PBZT Trimer.* The apparent global energy minimum for t-DBZT, PBZT dimer, and PBZT trimer five-molecule aggregates are given in Table 2. The geometry of each of these global energy minima is represented in Figures 6 and 7. For the t-DBZT global minima in Table 2, the coulomb contribution to the total energy is less than 4%. Similarly the intramolecular term is small, less than 2%. The total energy is thus dominated by the nonbonding term as found in most other structures.[6] The very close van der Waals contact of the molecules in Figure 6 is characteristic of all the minima in Table 2. Among the 700 local minima generated for t-DBZT in the simulation, 31 distinct orders were found within 5 kcal of the global energy minimum. The predicted dihedral angles ϕ_1 and ϕ_2 (cf. Figure 2a) for the global energy minimum structure are 6.55 and 7.72°, respectively. The values of E_T in Table 2 are much larger than the energy barrier to rotation about the C4–C5 and C22–C23 bonds (which is on the order of 2 kcal/mol of C–C bonds[16]). The values of ϕ_1 and ϕ_2 are thus more likely to be determined by intermolecular interactions than intramolecular interactions, and as we see here the structure remains relatively planar in these aggregates.

Apart from considering t-DBZT as a model of the PBZT polymer, it was of interest to us to determine how well the Monte Carlo predictions approximated the real translation aggregates of t-DBZT. There are two known crystal forms of this compound. One X-ray crystal structure (structure I) has been reported previously,[12] and the second (structure II) is reported here for the first time in Appendix A. The predicted structures which are closest to the experimental data are given in Table 3. In structure I the lowest one dimensional aggregate is actually a *translation* aggregate of two symmetry-independent molecules rather than the one molecule assumed in the simulation. This accounts for the difference between the global minimum and structure I (7.84 kcal; a structure is usually found within 5 kcal of the global energy minimum[6]), and it is gratifying

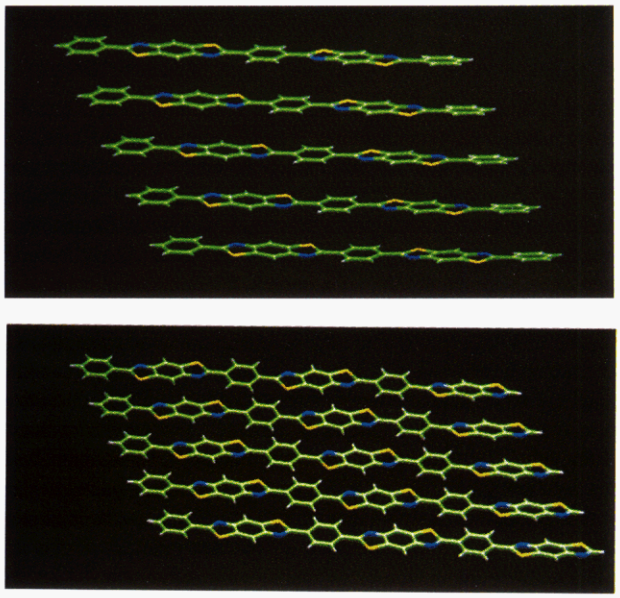

Figure 7. Five molecule translation aggregates with global energy minimum geomtries for (a, top) PBZT dimer (translation repeat = 3.88 Å) and (b, bottom) PBZT trimer (translation repeat = 4.00 Å), viewed along the stacking direction.

Table 3. Structures Determined in Monte Carlo Simulations Which Are Closest in Geometry to Aggregates in Real Crystal Structures of t-DBZT and PBZT

	θ_{iz}[a] $\Delta\theta_{iz}$[e]	θ_{jz}[a] $\Delta\theta_{jz}$[e]	θ_{kz}[a] $\Delta\theta_{kz}$[e]	t[b] Δt[e]	ΔE_T[c]	RSS[d]
I[f]	94.71	36.55	53.86	5.93	3.71	15.26
	8.04	2.18	−1.98	−0.70		
II[g]	77.41	34.17	121.17	6.34	7.84	23.25
	12.94	3.86	15.94	0.57		
III[h]	95.84	91.02	5.93	3.64	3.74	2.22
	0.90	0.11	0.87	0.10		
IV[i]	96.87	91.54	7.04	3.66	4.99	2.88
	0.13	0.63	0.24	0.12		

[a] Tilt angle (in degrees) in the i, j, or k direction (rotating axes) with respect to the z axis (stationary). [b] Translation repeat distance (along the z axis) in angstroms. [c] Difference in energy between the predicted structure and the global energy minimum. [d] Root-sum square of differences in tilt angles and translation distance. [e] Difference between predicted and actual structures. [f] Predicted t-DBZT structure closest to that reported in ref 12. [g] Predicted t-DBZT structure closest to that reported in Appendix A. [h] Predicted PBZT dimer structure closest to that reported in ref 13 for PBZT. [i] Predicted PBZT trimer structure closest to that reported in ref 13 for PBZT.

to know that the method still has some success even when such complications arise. Structure II reported here (from Appendix A) matches well with a minimum only 3.71 kcal from the global energy minimum.

For the dimer and trimer, the Coulomb and intramolecular terms are also small (less than 4% of total energy) compared with the nonbonding contributions. Although there are significant twists from coplanarity in the molecular backbones of the *single* molecule energy minimized structures of the dimer and trimer, packing tends to flatten the structures (see Figure 7). The twist angles were on average less than 10°. For the PBZT trimer global minimum, ϕ was 8.3° on average. The E_{intra} terms show that achievement of these planar structures involves little expense in energy compared to the total, E_T. Thus, as was found for t-DBZT, intermolecular rather than intramolecular interactions are the dominant forces which determine the dihedral angles (ϕ): 28 orders were found for the dimer and 22 for the trimer within 5 kcal of the respective global energy minima. The local minima structures for the dimer predict a perpendicular interchain spacing Z in the range 3.36–3.59 Å where

$$Z = t \cos \theta_{kz} \tag{9}$$

For the PBZT trimer, Z is in the range 3.36–3.49 Å. Thus the tight chain packing evident in t-DBZT (Z = 3.41 Å for the global energy minimum structure in Figure 6) is also predicted for PBZT. These values are very close to the interchain spacing in the polymer which has been experimentally measured many times to be 3.50–3.54 Å.[1,12,26-28] In Table 3 we include comparisons of our calculations for the PBZT dimer and trimer with the lowest energy aggregate in the most recently reported crystal structure for PBZT.[13] Both the dimer and the trimer give very close fits to the observed structure, i.e., the deviations in tilt angles and translation distance are very small, and each structure is within 5 kcal of the global energy minimum.

Several years ago Mark and co-workers[18b] carried out some calculations on intermolecular interactions in PBZT. It is interesting to compare our results with their work. Their model for PBZT was based on interactions between a single repeat unit of PBZT with an adjacent chain with four repeat units and neglecting chain rotations. Interestingly, they were still able to locate an approximate energy minimum for a three-dimensional assembly of PBZT which has some of the characteristics of crystalline PBZT (they calculated Z = 3.5 Å). There are of course many other significant energy minima other than just the global minimum (indeed neither PBZT nor t-DBZT assume their global energy minimum structures in real crystals), and mutual intermolecular rotations and all intramolecular packing dimensions need to be considered in locating them.

(*B*) *$AlCl_3$ Complexes.* The global energy minimum for the *translation*, *glide*, *screw*, and *inversion* aggregates for the 1:4 t-DBZT:$AlCl_3$ complex are given in Table 4 and the global energy minima are represented in Figure 8. The Coulomb terms are larger than observed for the uncomplexed t-DBZT, accounting for up to 14% of total energy. Large intermolecular voids evident in Figure 8a for the global minimum were seen in all low-energy *translation* aggregate structure for this complex. Some of these voids have a diameter as large as a carbon atom (3.5 Å). The very tightly packed structures of t-DBZT are here replaced by structures with large intermolecular translation distances. The perpendicular distance Z between molecules ranges from 5.33 to 6.00 Å for the 10 lowest orders of the *translation* aggregate.

Two rows of the direction cosine matrix are included for the glide, screw, and inversion structures since one row, sufficient for description of the *translation* aggregate, does not suffice here.[6b] For the glide aggregate (Figure 8b), the two red molecules are identical by symmetry. The blue molecule is related to each by reflection in a mirror

(26) Roche, E. J.; Takahashi, T.; Thomas, E. L. In *Fiber Diffraction Methods*; French, A. D., Gardner, K. H., Eds.; American Chemical Society Symposium Series No. 141, 1980; pp 303–313.
(27) Odell, J. A.; Keller, A.; Atkins, E. D. T.; Miles, M. J. *J. Mater. Sci.* **1981**, *16*, 3309–3318.
(28) Cohen, Y.; Thomas, E. L. *Mol. Cryst. Liq. Cryst.* **1987**, *153*, 375–384.
(29) Hinze, J.; Jaffe, H. H. *J. Am. Chem. Soc.* **1962**, *84*, 540–546.
(30) Dalgarno, A. *Adv. Phys.* **1962**, *11*, 281–315.
(31) Teachout, R. R.; Pack, R. T. *At. Data* **1971**, *3*, 195–214.
(32) Hirschfelder, J. O.; Curtiss, C. F.; Bird, R. B. *Molecular Theory of Gases and Liquids*; John Wiley: New York, 1954; pp 951–955.
(33) Pitzer, K. S. *Adv. Chem. Phys.* **1959**, *2*, 59–83.
(34) Allen, F. H.; Kennard, O.; Taylor, R. *Acc. Chem. Res.* **1983**, *16*, 146. X-ray structure taken from the Cambridge Crystallographic Database, available from the Cambridge Crystallographic Data Centre, 12 Union Road, Cambridge CB2 1EW, U.K.

Table 4. Translation, Glide, Screw, and Inversion Aggregate Geometries and Lowest Energies for 1:4 t-DBZT:$AlCl_3$ Complex and 1:8 PBZT Dimer: $AlCl_3$ Complex

	θ_{iz}[a] θ_{ix}[b]	θ_{jz}[a] θ_{jx}[b]	θ_{kz}[a] θ_{kx}[b]	offset[c]	t[d] t_1[e]	E_{nb}[f]	E_{el}[f]	E_T[f]
1:4 t-DBZT:$AlCl_3$ Complex								
translation	116.35	91.64	26.41		6.70	−18.62	−0.24	−18.86
glide	158.95	68.95	90.18	−2.16	12.88	−24.35	−4.24	−28.59
	90.05	89.64	0.51					
screw	135.66	85.19	133.93	−3.49	8.99	−29.58	−2.27	−31.85
	53.62	116.87	131.77					
inversion	130.43	90.75	139.56	4.00	7.59	−30.41	−4.60	−35.01
	44.12	110.05	127.29		6.66			
1:8 PBZT Dimer:$AlCl_3$ Complex								
translation	85.82	57.56	32.47		6.87	−46.09	5.01	−41.08

[a] Tilt angle (degrees) in the i, j, or k direction (rotating axes) with respect to the z axis (stationary axis). [b] Tilt angle (in degrees) in the i, j, or k direction (rotating axes) with respect to the stationary x axis (not needed for the translation aggregate). [c] Offset distance in angstroms (not needed for the translation aggregate). [d] Repeat distance between successive molecules related by translation symmetry. [e] One of the translation distances in angstroms between successive inversion related molecules. The other is $t_2 = t - t_1$. [f] Energy in kcal/mol as defined by eq 1.

plane, an offset vertically from the translation axis, and a translation $t/2$. Although the *glide*, *screw* and *inversion* structures of Table 4 are of lower energy than the *translation* aggregate, the molecules still pack inefficiently, leaving large voids in the aggregate structures which cannot be filled by atoms on adjacent molecules. For example, in the view of the global energy minimum for the *glide* aggregate in Figure 8b, the distance between molecular centers of the two red molecules is the repeat distance 12.88 Å. Since these molecules lie almost flat in the xy plane ($\theta_{kz} = 90.18°$), Z is approximately zero and the other tilt angles are such as to give a shift in the Y, or long molecular axis, direction of 4.63 Å and an X direction separation of 12.02 Å. The visible result of this is the empty channel along the molecular axis between each such pair of molecules. Similar cavities were visible in the low energy *screw* aggregate structures. For example in Figure 8c for the *screw* aggregate global minimum such cavities are visible between adjacent $AlCl_3$ moieties on each molecule. In the view shown the red molecule is superimposed on a symmetrically identical molecule which is translated along the z axis by 8.99 Å.

For the *inversion* aggregate the energies are computed from seven-molecule aggregates instead of five because of the importance of energy contributions from extra molecules in *inversion* aggregates.[6b] The geometry of the global energy minimum is shown in Figure 8d. The *inversion* aggregates are constructed as follows:[6b] A single molecule, appropriately oriented is used to make the next molecule by inversion of its coordinates. These two molecules are offset along the x axis, and the replicate is translated along the z axis by a distance t_1. A third molecule is constructed by inverting the coordinates of the second, offsetting along x and translating by a distance t_2 along the z axis. The process is repeated to generate further molecules in an aggregate. As observed in the other aggregates, large cavities unfillable by other molecules are evident in Figure 8d for the global energy minimum aggregate. Clearly the channels between the top red molecule and the blue molecule below and to the left, and similarly between the bottom red molecule and the blue molecule above and to the right, will not be filled. When this aggregate is viewed from above, as in Figure 8e where symmetrically identical blue and red molecules are superimposed, an unfilled hole is evident in the center of the structure.

The simulation results for the lowest energy *translation* aggregate of the 1:8 PBZT dimer:$AlCl_3$ complex are also given in Table 4. Of the 350 local minima generated, all but 60 were classified into order zero, the global energy minimum. Since the results for the 1:4 t-DBZT:$AlCl_3$ complex showed that similar packing inefficiencies were evident for all four symmetry types, we therefore present results here only for the *translation* aggregates of the dimer complex. Two representations of the global energy minimum are given in Figure 9. This minimum is formed by a separation Z of 5.80 Å perpendicular to the plane of the benzobisthiazole rings and a tilt angle of 57.56° in the y direction producing an axial shift of 3.69 Å. There is also a small shift (0.50 Å) in the x direction. The result of this packing is a large intermolecular cavity between adjacent molecules in the aggregate, similar to the *translation* aggregates for the 1:4 t-DBZT:$AlCl_3$ complex. In contrast to the aggregates of the 1:4 t-DBZT:$AlCl_3$ complex, the PBZT dimer complex has very few structures which can readily be adopted.

Discussion

In this paper we have modeled PBZT and its Lewis acid complexes with various oligomers and oligomer complexes. This imposes several approximations to reality. First, we have used molecules with 1–3 repeat units to model real molecules which generally contain greater than 100. Second, we have assumed an idealized view of the complexation process wherein every possible Lewis base site in the structure is coordinated by one Lewis acid. Although this picture is basically correct,[1] the complicating effects of any chain defects, isolated uncomplexed sites, end groups, and heterolysis of the Lewis acid (dissociation of chloride ions) which occurs in very dilute solution, have been ignored. However, these models help explain the observed effects of complexation on the properties of PBZT and give useful insight into their structural details.

The single-molecule energy-minimized structures of t-DBZT, the PBZT dimer, and trimer were shown to approximate very well the linear structure and the repeat unit dimensions actually observed for t-DBZT and PBZT. This gives us some confidence in our ability to make predictions for structures of PBZT complexes from similar models of oligomer complexes. The most obvious effect of complexation by $AlCl_3$ is that the molecular backbone becomes sterically congested and, as a result, nonplanar. The molecular shape is altered such as to increase the average chain diameter because the Lewis acids resemble bulky side groups on the main chain. The rigid-rod nature of PBZT is clearly retained in the complexes, as is confirmed by the observed high intrinsic viscosities[1,35] and liquid crystallinity[1,36] at high concentrations in solution.

Electron transfer from the electron-rich N and S heteroatoms to the electron-poor aluminum is predicted by the ESP calculations and gives a semiquantitative picture of the Lewis acid–base reactions. Complexation of the nitrogens is predicted to be strong because of the

(35) (a) Jenekhe, S. A.; Johnson, P. O.; Agrawal, A. K. *Macromolecules* **1989**, *22*, 3216–3222. (b) Jenekhe, S. A.; Johnson, P. L. *Macromolecules* **1990**, *23*, 4419–4429.

(36) Roberts, M. F.; Jenekhe, S. A. *Polym. Commun.* **1990**, *31*, 215–217.

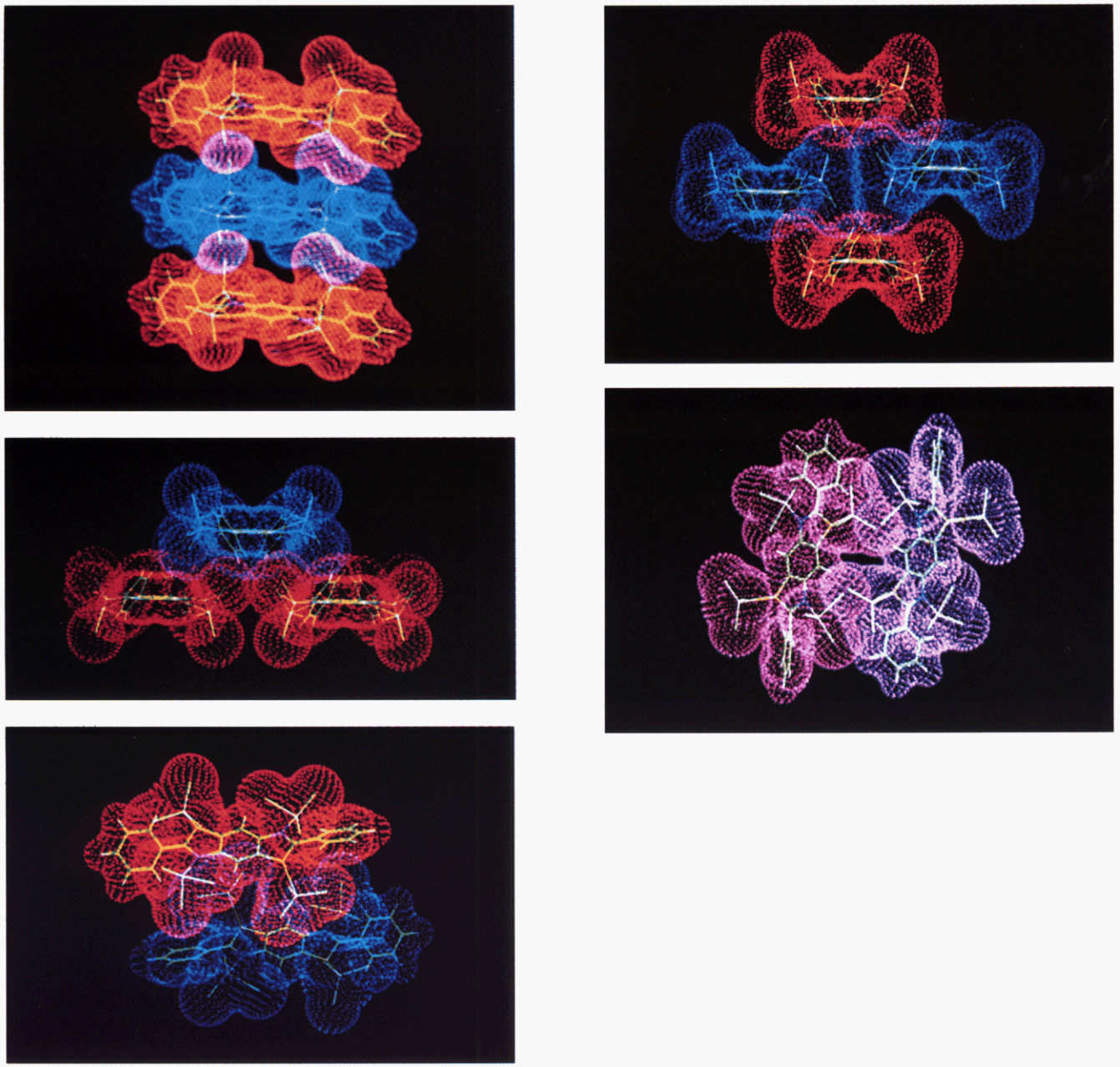

Figure 8. Global energy minimum aggregate geometries for the 1:4 t-DBZT:$AlCl_3$ complex: (a, top left) three molecules of the translation aggregate (translation repeat = 6.70 Å vertical); (b, middle left) three molecules of the glide aggregate (translation repeat = 12.88 Å horizontally and offset = 2.16 Å, vertically); (c, bottom left) three molecules of the screw aggregate viewed down the translation repeat axis (translation repeat = 8.99 Å into the plane of the page, and offset = 3.49 Å vertically); (d, top right) four molecules of the inversion aggregate; (e, bottom right) inversion aggregate of (d) viewed in a plane perpendicular to the translation repeat direction (offset = 4.00 Å, horizontally).

high degree of charge transfer and sulfur is predicted to be only weakly complexed by the same measure. This is further supported by the predicted shorter N–Al (1.90 Å) bonds compared to S–Al (2.59 Å) and the greater distortion of $AlCl_3$ from triangular planarity at the nitrogens. The charge redistributions predicted on complexation result in a greatly increased molecular dipole moment of complexed t-DBZT, and by extension, of PBZT complexes. Experimental observations support that this is in fact the case. PBZT complexes with $AlCl_3$ and $GaCl_3$ are soluble in highly polar solvents (high dielectric constant and dipole moment) with low electron-donating ability (low donor number) such as the nitroalkanes. However, chlorinated hydrocarbons such as dichloromethane and dichloroethane which have even lower donor numbers than nitroalkanes are not good solvents for PBZT complexes because of their lower polarities.

The effects of complexation on electronic structure, as measured by optical absorption spectra, can be rationalized on the basis of the INDO/S calculations. A blue-shift due to steric congestion which is caused by coordination of the Lewis acid is compensated for by a red-shift due to π-electron redistribution. The net effect is that complexation does not significantly change the position (λ_{max} and E_g) of the main π-electron absorption band.

Aggregate structure calculations for t-DBZT accurately predict the observed one-dimensional aggregate structures of t-DBZT in real crystals. The PBZT dimer and trimer models gave excellent fits to the observed crystal structure[12,26–28] of PBZT. It is very interesting that we can model a two-dimensional layer of PBZT (the second dimension being the molecular axis) successfully by considering the one-dimensional aggregate structure of only two or three repeat units. The PBZT structures which

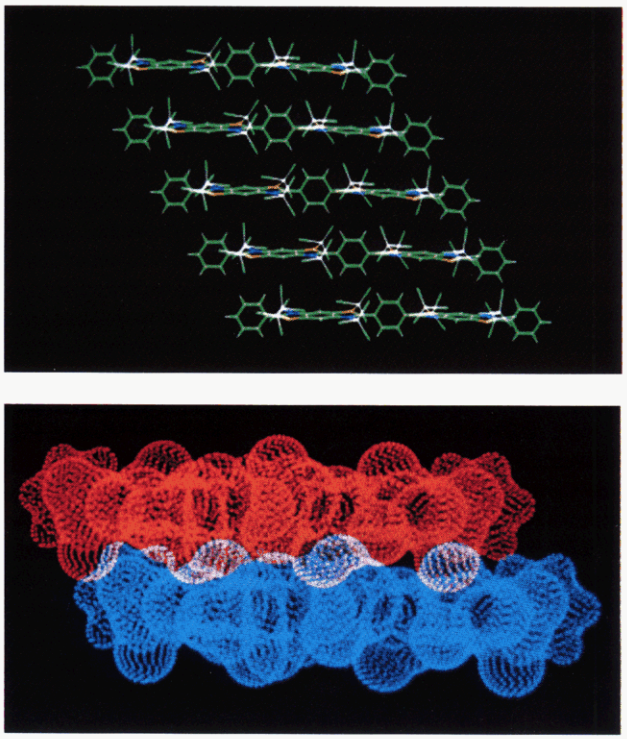

Figure 9. Translation aggregate global energy minimum for the 1:8 PBZT dimer:$AlCl_3$ complex: (a, top) five-molecule stick representation; (b, bottom) two molecule Connolly surface representation. Both views are along the stacking direction (translation repeat = 6.87 Å).

we obtain exhibit minimal intermolecular free volume and should have very high cohesive energy densities (CEDs).[37] Both factors are known[37,38] to influence polymer solubility and glass transition temperature and coupled with the rigid-rod nature of the individual polymer molecules, these factors together result in the intractability and insolubility that is characteristic of PBZT.

On the other hand, the predicted aggregate structures of PBZT oligomer complexes exhibit very inefficient packing of the chains with unfillable intermolecular voids and cavities. It is not possible to quantify free-volume fractions or CED with the present results due first to the fact that we are studying one-dimensional aggregates instead of the more complicated two-dimensional layer structures[9] which for PBZT would approximate three-dimensional assemblies. Second, there are inaccuracies in the energy model arising not only from the approximated nonbonding parameters for aluminum but also from the MM2 model[4] and the Gasteiger model.[14] Thus, although we can predict aggregate geomtries confidently, the intermolecular energies are probably inaccurate. Despite these limitations, there are several useful insights into the effects of complexation on free volume and CED to be gained from the results.

In previous papers we have discussed how PBZT may be solubilized in organic solvents as its complexes with various Lewis acids. This discovery ends a long search for viable organic solvent systems for the solubilization and processing of PBZT into films, coatings, and fibers.[35,36] The question arises as to what is the means by which such complexation reactions lead to solubilization of PBZT in organic solvents to which the polymer was previously completely resistant. An answer to this lies in the present aggregate structure calculations. What we find is that complexes of PBZT oligomers (t-DBZT and the dimer) find it very difficult to form efficiently packed aggregate structures. Comparing *translation* aggregates of the oligomers with those of the complexes, we see that aggregates of the complexes have much larger free volume fractions. Interchain distances, Z, for t-DBZT, the dimer and the trimer are on the order of 3.3–3.5 Å which increases to 5.3–6.0 Å in the complexes with most of the intervening volume free. At the same time there are no large increases in intermolecular energy. *Glide*, *screw*, and *inversion* aggregates exhibit analogously large free volume fractions. The result of complexation must therefore be decreased CEDs. Van Krevelen[37] has discussed CED, or more specifically the solubility parameter which is the square root of CED, and its relationship to polymer solubility. It is at least qualitatively clear that any process which decreases the CED of an intractable polymer such as PBZT will thereby enhance its solubility. Others,[39] for example, have covalently attached flexible or bulky side groups to rigid-chain polymers to improve solubility and processability at the expense of permanently altering polymer properties for the worse. We conclude that Lewis acid complexation reduces the CED of PBZT, and this accounts for the dramatic improvements in solubility.

We have also reported that PBZT/Lewis acid complexes form liquid-crystalline solutions in organic solvents with significantly higher critical concentrations (C_{cr}) than observed with protonic acid solutions.[1,36] C_{cr} for PBZT in $AlCl_3$/nitromethane is 5 wt % and in $GaCl_3$/nitromethane it is 8 wt %, while in MSA it is only 4 wt %. These increases in C_{cr} may also be explained by the present results. Complexes of PBZT oligomers have larger average chain diameters and pack with much larger interchain distances in the nonaxial directions in aggregates. The net result is decreased effective molecular axial ratios (ratio of chain length to average chain diameter). By extension we expect this to be the case in lyotropic solutions of PBZT complexes. Lattice theory predictions[40] are that decreased axial ratios lead to increased critical concentrations. We conclude that Lewis acid complexes of PBZT have smaller effective axial ratios than PBZT has in MSA solutions and this leads to their observed higher critical concentrations.

Another result of complexation of PBZT with Lewis acids is the observation that the PBZT/$GaCl_3$ complex is a stable solid with a glass transition (T_g) close to room temperature.[1] By contrast, PBZT exhibits no discernible T_g below the decomposition temperatures (650–700 °C). From free volume theory,[41] T_g should decrease with increasing free volume in polymers. T_g has also been correlated with and found to decrease with decreasing CED.[37,38] The effect of complexation on T_g must therefore be due to a combination of both factors, since in the oligomer complex aggregates both effects are evident. Of course we are interpreting a phenomenon observed in an amorphous polymer complex in light of simulations with crystalline oligomer aggregates. The question of the structure of amorphous polymers is still hotly debated[38] since it is not clear whether in amorphous polymers there

(37) Van Krevelen, D. W. *Properties of Polymers*, 2nd ed.; Elsevier Scientific Publishing Co.: New York, 1976; pp 99–172.
(38) Boyer, R. F. In *Computational Modeling of Polymers*; Bicerano, J., Ed.; Marcel Dekker Inc.: New York, 1992; pp 1–52.
(39) Postema, A. R.; Liou, K. R.; Wudl, F.; Smith, P. *Macromolecules* **1990**, *23*, 1842–1845.
(40) Flory, P. J. *Adv. Polym. Sci.* **1984**, *59*, 1–35.
(41) McCrum, N. G.; Read, B. E.; Williams, G. *Anelastic and Dielectric Effects in Polymer Solids*; Dover Publications Inc.: New York, 1991; pp 169–174.

is a completely random molecular arrangement or a random assembly of regions of local order. What we can say is the following: We expect crystalline arrays of molecules to be the most efficiently packed arrangements. PBZT oligomer complexes exhibit aggregate packing arrangements of large free volume fraction and low CED compared to PBZT oligomers. Consequently amorphous PBZT complexes, because they are more randomly and therefore less efficiently packed than crystalline oligomer complex aggregates, should have even larger free volume fractions and lower CEDs.

Conclusions

Two basic questions were posed in the introduction of this paper. The first of these was, what are the effects of Lewis acid complexation on the molecular structure, conformation, and electronic structure of PBZT? We find that the molecular structures of the complexes are highly linear with the same overall rigid-rod conformation as the pure PBZT. However, coordination of the Lewis acid causes steric congestion about the heteroatoms, the net result being a highly nonplanar molecular structure due to large out-of-plane twists of the phenylene rings. The coordinated Lewis acids resemble bulky side groups and increase the effective molecular diameter of PBZT. There is electron transfer from each of the coordinated nitrogens and sulfurs to aluminum, confirming the underlying Lewis acid–base type reaction of the complexation. Sulfur is found to be less basic than nitrogen in this respect. Electron redistribution causes a large increase in the molecular dipole moment when PBZT is complexed. There are two opposing effects of complexation on the π–π^* absorption band of PBZT. One is a blue-shift due to the induced molecular nonplanarity which inhibits π-electron delocalization. The other is a red-shift which results from π-electron redistribution. The two effects produce a very small net effect on the position of the π–π^* absorption band.

The second question addressed was, how does structure account for the observed solution- and solid-state properties of PBZT complexes? The computational modeling results suggest that the solubility of PBZT complexes in organic solvents is due to reduced cohesive energy density compared to the pure polymer. The smaller cohesive energy density arises from packing inefficiencies of the complexed polymer chains. Solubility in polar organic solvents is aided by the increased molecular dipole moment of PBZT when it is complexed. Complexation increases the critical concentration for anisotropic phase separation of PBZT in solution by increasing the average molecular diameter and thereby decreasing the axial ratio. The large free volume fractions in aggregates of the complexes and the reduced cohesive energy density are also responsible for the extremely low glass transition temperature exhibited by the PBZT/$GaCl_3$ complex.

Acknowledgment. This research was supported in part by the National Science Foundation (CTS-9311741), the NSF Center for Photoinduced Charge Transfer (CHE-9120001), and an Elon Huntington Hooker Fellowship to MFR.

Supplementary Material Available: Coordinates for the MM2 geometry and ESP charges, refinement data, and thermal parameters (13 pages); observed and calculated structure factors (1 page). Ordering information is given on any current masthead page.

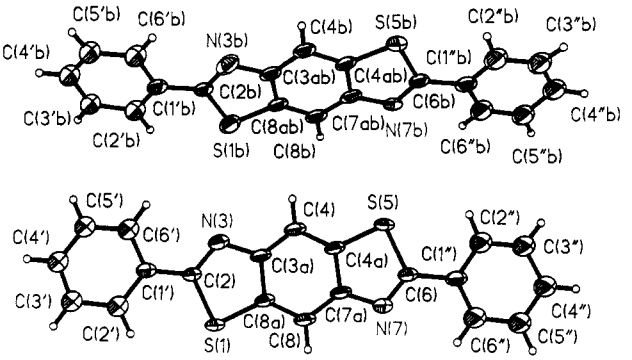

Figure 10. Structure of t-DBZT showing thermal ellipsoids at 50% probability.

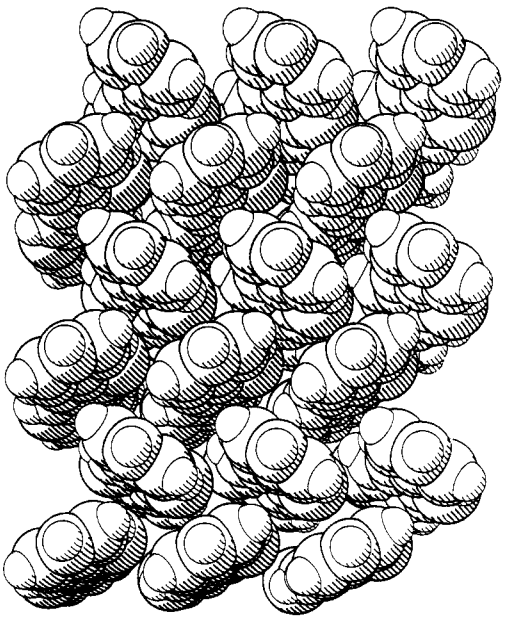

Figure 11. Space-filling representation of hexagonal close packed (001) face of t-DBZT.

Appendix A. Crystal Structure and Molecular Packing of t-DBZT

We have determined the crystal structure and molecular packing of the new P1 polymorph of 2,6-diphenylbenzo-[1,2-*d*:4,5-*d'*]bisthiazole (t-DBZT) by X-ray crystallography (Figure 10). The triclinic cell contains two molecules of t-DBZT which are aligned parallel at an orientation of 52.6° relative to each other with the long molecular axis pointing along [001]. The relative displacement is only about 1.5 Å. This alignment gives rise to molecular hexagonal close packing (HCP) in the (001) plane (Figure 11) resulting in molecular sheets of t-DBZT which are stacked to give the third packing dimension in the crystal (Figure 12). The crystal habit is a very high aspect ratio thin tablet with the (001) face being prominent. This observation is consistent with two-dimensional HCP.

The t-DBZT was kindly provided to us by the Air Force Materials Laboratory, Dayton, OH. The sample was recrystallized from toluene to form the high aspect ratio crystals. Elemental analysis was carried out by Galbraith Laboratories, Knoxville TN. The expected composition for $C_{20}H_{12}N_2S_2$ is 69.77% C, 3.52% H, 8.14% N, and 18.64% S. We obtained 69.60% C, 3.71% H, 7.92% N, and 19.35% S. The dimensions of the selected crystal

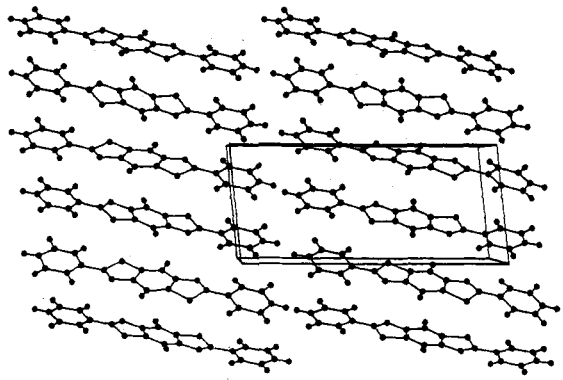

Figure 12. View along [100] of t-DBZT showing layering along [001].

Table 5. Crystal Data for t-DBZT

compound	2,6-diphenylbenzo[1,2-*d*:4,5-*d'*]-bisthiazole (PBZT)
formula	$C_{20}H_{12}S_2N_2$
formula wt	344.5
crystal system:	triclinic
space group (No.)	*P*1 (1)
Z (molecules/unit cell)	2
a (Å)	5.771(4)
b (Å)	7.863(3)
c (Å)	17.32(1)
α, deg	84.03(4)
β, deg	86.09(6)
γ, deg	88.90(4)
V (Å^3)	780(4)
density calcd (g/cm^3)	1.47(1)
habit	high aspect ratio thin plates
size (mm)	0.4 × 0.4 × 0.03
color	translucent white

were 0.4 × 0.4 × 0.03 mm. Data were collected on an Enraf Nonius Cad-4 diffractometer using graphite monochromated Cu Kα radiation and the ω–2θ scan mode. Although approximate lattice constants were obtained by precession photography, the final cell (Table 5) was determined on the diffractometer from least-squares fitting of the angular settings of 25 reflections well distributed in reciprocal space. Three reference reflections were collected periodically for intensity and orientation control, and a half-sphere of data was taken to a resolution of 0.95 Å (55° θ). Reflection profiles were collected, and the Bragg peak profiles were processed using the DREAM data reduction package[42] to give the intensity and variance for each reflection. After appropriate scaling and merging the data were subjected to a Bayesian statistical treatment[44] to get a better estimate of the intensities and standard deviations of the weak and unobserved reflections. A total of 2577 reflections were output as F_{obs} and $\sigma(F_{obs})$ with $F/\sigma > 0$.

The structure was solved by direct methods using the SHELXTL package[45] with $|E| > 1.2$. The *E* statistics gave rise to a hypercentric distribution, but the *E* map clearly showed all of the non-hydrogen atoms of both molecules with a relative orientation such that there could be no inversion center. The space group was assigned *P*1.

No absorption correction was made and therefore many of the thermal parameters became unphysical during the course of the refinement. To get reasonable thermal parameters, chemically equivalent atoms on both molecules were refined with one set of parameters (except the

Table 6. Atomic Coordinates for Two Molecules of t-DBZT Unit Cell

	x/a	*y/b*	*z/c*	U_{eq}	occ
			Molecule 1		
S1	1.519(0)	1.271(0)	0.792(0)	0.051(1)	1.000(0)
C2	1.282(2)	1.207(1)	0.858(1)	0.042(1)	1.000(0)
N3	1.110(2)	1.135(1)	0.827(1)	0.047(3)	1.000(0)
C3A	1.160(2)	1.122(1)	0.748(1)	0.042(1)	1.000(0)
C4	1.008(2)	1.060(1)	0.700(1)	0.045(1)	1.000(0)
H4A	0.864(2)	1.009(1)	0.720(1)	0.000(0)	1.000(0)
C4A	1.086(2)	1.056(1)	0.623(1)	0.042(1)	1.000(0)
S5	0.944(0)	0.985(0)	0.548(0)	0.046(1)	1.000(0)
C6	1.182(2)	1.048(1)	0.484(1)	0.042(1)	1.000(0)
N7	1.345(2)	1.118(1)	0.513(1)	0.047(3)	1.000(0)
C7A	1.300(2)	1.128(1)	0.591(1)	0.042(1)	1.000(0)
C8	1.447(2)	1.201(1)	0.640(1)	0.045(1)	1.000(0)
H8A	1.601(2)	1.237(1)	0.621(1)	0.000(0)	1.000(0)
C8A	1.377(2)	1.193(1)	0.719(1)	0.042(1)	1.000(0)
C1′	1.271(2)	1.249(1)	0.937(1)	0.045(1)	1.000(0)
C2′	1.453(2)	1.338(2)	0.966(1)	0.061(1)	1.000(0)
H2′A	1.583(2)	1.372(2)	0.931(1)	0.000(0)	1.000(0)
C3′	1.437(2)	1.378(2)	1.045(1)	0.061(1)	1.000(0)
H3′A	1.564(2)	1.438(2)	1.063(1)	0.000(0)	1.000(0)
C4′	1.254(2)	1.319(2)	1.090(1)	0.061(1)	1.000(0)
H4′A	1.243(2)	1.351(2)	1.142(1)	0.000(0)	1.000(0)
C5′	1.077(2)	1.232(2)	1.064(1)	0.061(1)	1.000(0)
H5′A	0.956(2)	1.185(2)	1.100(1)	0.000(0)	1.000(0)
C6′	1.080(2)	1.191(2)	0.989(1)	0.061(1)	1.000(0)
H6′A	0.948(2)	1.140(2)	0.970(1)	0.000(0)	1.000(0)
C1″	1.187(2)	1.008(1)	0.401(1)	0.045(1)	1.000(0)
C2″	1.009(3)	0.917(2)	0.376(1)	0.061(1)	1.000(0)
H2″A	0.873(3)	0.881(2)	0.409(1)	0.000(0)	1.000(0)
C3″	1.014(2)	0.881(2)	0.301(1)	0.061(1)	1.000(0)
H3″A	0.907(2)	0.804(2)	0.283(1)	0.000(0)	1.000(0)
C4″	1.202(2)	0.931(2)	0.246(1)	0.061(1)	1.000(0)
H4″A	1.200(2)	0.914(2)	0.192(1)	0.000(0)	1.000(0)
C5″	1.378(2)	1.029(2)	0.272(1)	0.061(1)	1.000(0)
H5″A	1.508(2)	1.066(2)	0.237(1)	0.000(0)	1.000(0)
C6″	1.368(2)	1.060(2)	0.351(1)	0.061(1)	1.000(0)
H6″A	1.487(2)	1.128(2)	0.368(1)	0.000(0)	1.000(0)
			Molecule 2		
S1B	0.015(1)	0.602(0)	0.816(0)	0.052(1)	1.000(0)
C2B	−0.221(2)	0.718(1)	0.856(1)	0.042(1)	1.000(0)
N3B	−0.389(2)	0.755(1)	0.810(1)	0.054(3)	1.000(0)
C3AB	−0.340(2)	0.700(1)	0.738(1)	0.042(1)	1.000(0)
C4B	−0.491(2)	0.721(1)	0.679(1)	0.045(1)	1.000(0)
H4BA	−0.640(2)	0.776(1)	0.683(1)	0.000(0)	1.000(0)
C4AB	−0.416(2)	0.648(1)	0.610(1)	0.042(1)	1.000(0)
S5B	−0.551(1)	0.654(0)	0.525(0)	0.051(1)	1.000(0)
C6B	−0.318(2)	0.541(1)	0.485(1)	0.042(1)	1.000(0)
N7B	−0.151(2)	0.497(1)	0.529(1)	0.043(3)	1.000(0)
C7AB	−0.198(2)	0.560(1)	0.602(1)	0.042(1)	1.000(0)
C8B	−0.053(2)	0.538(1)	0.663(1)	0.045(1)	1.000(0)
H8BA	0.092(2)	0.477(1)	0.658(1)	0.000(0)	1.000(0)
C8AB	−0.130(2)	0.609(1)	0.730(1)	0.042(1)	1.000(0)
C1′B	−0.225(2)	0.752(1)	0.937(1)	0.045(1)	1.000(0)
C2′B	−0.052(2)	0.700(2)	0.986(1)	0.061(1)	1.000(0)
H2′B	0.080(2)	0.640(2)	0.964(1)	0.000(0)	1.000(0)
C3′B	−0.080(2)	0.737(1)	1.066(1)	0.061(1)	1.000(0)
H3′B	0.041(2)	0.692(1)	1.098(1)	0.000(0)	1.000(0)
C4′B	−0.274(2)	0.826(2)	1.090(1)	0.061(1)	1.000(0)
H4′B	−0.279(2)	0.843(2)	1.145(1)	0.000(0)	1.000(0)
C5′B	−0.433(2)	0.883(2)	1.043(1)	0.061(1)	1.000(0)
H5′B	−0.558(2)	0.951(2)	1.064(1)	0.000(0)	1.000(0)
C6′B	−0.422(2)	0.846(2)	0.965(1)	0.061(1)	1.000(0)
H6′B	−0.543(2)	0.882(2)	0.931(1)	0.000(0)	1.000(0)
C1″B	−0.306(2)	0.497(1)	0.403(1)	0.045(1)	1.000(0)
C2″B	−0.481(2)	0.555(2)	0.355(1)	0.061(1)	1.000(0)
H2″B	−0.617(2)	0.614(2)	0.374(1)	0.000(0)	1.000(0)
C3″B	−0.471(2)	0.529(2)	0.279(1)	0.061(1)	1.000(0)
H3″B	−0.582(2)	0.572(2)	0.243(1)	0.000(0)	1.000(0)
C4″B	−0.297(2)	0.433(2)	0.247(1)	0.061(1)	1.000(0)
H4″B	−0.279(2)	0.407(2)	0.194(1)	0.000(0)	1.000(0)
C5″B	−0.110(2)	0.376(2)	0.296(1)	0.061(1)	1.000(0)
H5″B	0.019(2)	0.308(2)	0.278(1)	0.000(0)	1.000(0)
C6″B	−0.128(2)	0.406(2)	0.371(1)	0.061(1)	1.000(0)
H6″B	−0.008(2)	0.361(2)	0.404(1)	0.000(0)	1.000(0)

(42) (a) Blessing, R. H. *J. Appl. Crystallogr.* **1986**, *19*, 412. (b) Blessing, R. H. *Cryst. Rev.* **1986**, *1*, 3–58.
(43) McMillan, M.; Blessing, R. H. *J. Appl. Crystallogr.*, to be submitted.
(44) Wilson, K.; French, S. *Acta Crystallogr.* **1978**, *A34*, 517–525.
(45) Sheldrick, G. M. *Acta Crystallogr.* **1990**, *A46*, 467–473.

sulfurs and nitrogens). All of the carbons on the phenyl rings (except the C1 carbons) had the same set of thermal parameters. For these reasons, the residuals were not very low except for the goodness of fit (1.30). The data quality is good with 92% of the reflections having $F > 4\sigma$, and the refined parameters are chemically and physically sound. Figure 10 shows the final structure and Table 6 presents the coordinates for the two molecules in the asymmetric unit. The molecules are nearly planar with the phenyl groups making an angle of 6° on average with respect to the benzobisthiazole portion of the compound. Other researchers working with the $P2_1/c$ polymorph found 23° twist angles.[12] The structure of the cis isomer 2,6-diphenylbenzo[1,2-*d*:5,4-*d'*]bisthiazole published in the same paper is nearly planar, and it also has two molecules per asymmetric unit which make a dihedral angle of 53.4° relative to the benzobisthiazole frame. This value is essentially the same as the 52.6° angle found in this study.

Appendix B. Calculation of Gasteiger Parameters and Force Field Parameters for Aluminum Atoms

Use of the model described in this paper for energy computation requires parameters for calculation of nonbonded interactions (eq 2) and parameters for calculating partial atomic charges for Coulomb interactions (eq 6) for all the atoms present. These are available for all of the atoms needed (C, H, N, S, Cl)[4,14] except aluminum. We used the following approach to estimate the necessary values for aluminum.

The procedure described by Gasteiger and Marsili[14] was used to calculate the charge distribution for all molecules in the Monte Carlo simulations. A tetrahedral environment was assumed for aluminum since this is its approximate configuration in complexes with PBZT oligomers. The first step was to calculate parameters for the orbital electronegativity dependence on atomic charge:

$$\chi_{iv} = a_{iv} + b_{iv}Q_i + c_{iv}Q_i^2 \qquad \text{(B1)}$$

χ_{iv} is the orbital electronegativity of atom i, Q_i is its charge, and a_{iv}, b_{iv}, and c_{iv} are the desired parameters, calculated from reported ionization potentials and electron affinities.[29] For tetrahedral aluminum we calculated values of 5.38, 6.10, and 2.02, respectively. Calculation of charges from these parameters employs an iterative procedure[14] which has been incorporated into the simulation program.[6a]

Estimation of the nonbonding energy parameters for aluminum (A_i in eq 3 and B_i in eq 4) requires first the atomic polarizability, α. The polarizability of a metal atom such as aluminum varies widely with charge. For Al^{3+}, Dalgarno[30] reported a value of 0.05 and Teachout and Pack[31] compiled values of 5 and 11.0 from the literature for Al^0. We calculated values of 0.08 and 21.0 for Al^{3+} and Al^0, respectively, using screening constants.[32] These discrepancies between values obtained from different calculations and the large variation of α with atomic charge make it difficult to estimate α for aluminum as it occurs in the complexes. We settled on a value of 8.9 by averaging reported values and interpolating with an assumed charge of +0.58 on aluminum from a Gasteiger calculation for $AlCl_3$.

Next we employed the Slater–Kirkwood formula[22] to calculate an attractive force coefficient c_{ii} for aluminum. For two atoms i and j the formula is

$$c_{ij} = \frac{{}^3/_2 e(h/m^{1/2})\alpha_i\alpha_j}{(\alpha_i/N_i)^{1/2} + (\alpha_j/N_j)^{1/2}} \qquad \text{(B2)}$$

where e is the electronic charge, h is Planck's constant, and m is the electron rest mass. N, estimated from Pitzer's data,[33] is 12 for aluminum. Computation gave a value of 16 711 for c_{ii}. This parameter was used in the Buckingham force field of Scott and Scheraga,[22] which approximates the nonbonded energy between two atoms as follows:

$$E_{ij} = a_{ij}\exp(-b_{ij}r_{ij}) - c_{ij}/r_{ij}^6 \qquad \text{(B3)}$$

Units are to give energy in kcal/mol. The repulsive force constants a_{ij} and b_{ij}, estimated from their paper are 4.26×10^8 and 4.2, respectively. To calculate a_{ii} the van der Waals radius of aluminum was necessary and obtained from Bondi's tables[23] as 2.51 Å.

Finally we use the observation that eq B3 and eq 2 are similar in form to estimate the parameters A_i and B_i for aluminum. B_i is most easily estimated as just the van der Waals radius, 2.51 Å, and we approximate A_i as 0.464.

Clearly there is room for discrepancy in the calculated values of A_i and B_i. For A_i the main source of such errors is in the estimation of polarizability. Any error in B_i is due to the assumed van der Waals radius, which is difficult to estimate for metals.[23] However, our need here is to generate parameters which are sufficiently accurate to do the aggregate structure modeling. We carried out a test of the adequacy of the parameters by running a simulation for the complex I.

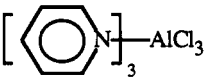

I

This molecule has been given the reference code BODZAV in the Cambridge Crystallographic Database.[34] The lowest energy one-dimensional aggregate in the crystal structure has translation symmetry with translation distance (t), and tilt angles with respect to the z axis θ_{iz}, θ_{jz}, and θ_{kz} of 7.26 Å, 118.3°, 63.6°, and 40.6°, respectively. A Monte Carlo simulation yielded a local energy minimum 2.14 kcal from the global energy minimum with respective values of 7.28 Å, 117.6°, 64.0°, and 39.6°. This geometry is very close (root-sum-square deviation (RSS) = 1.31) to that observed. On the basis of this result, we reason that the energy parameters we have calculated are at least good enough to accurately simulate aggregate geometries.